European Conference on Computational Fluid Dynamics
ECCOMAS CFD 2006
P. Wesseling, E. Oñate and J. Périaux (Eds)

LARGE-EDDY SIMULATION OF ISOTROPIC HOMOGENEOUS DECAYING TURBULENCE

Ben Thornber *, **Dimitris Drikakis** †

Department of Aerospace Sciences
Fluid Mechanics and Computational Science Group
Cranfield University, United Kingdom
*e-mail: b.j.r.thornber@cranfield.ac.uk,
† e-mail:d.drikakis@cranfield.ac.uk
web page: http://www.cranfield.ac.uk/soe/fluid/

Key words: LES, Implicit, Isotropic, Turbulence, Decay, MUSCL

Abstract. *Simulations of three dimensional freely decaying homogeneous turbulence in a periodic cube have been used to examine in a detailed and quantitative manner the behaviour of a Large Eddy Simulation (LES) using implicit subgrid modelling. This paper details the form and behaviour of the implicit subgrid models for the Minmod and third order limiting methods at several mesh resolutions. It is shown that for simulations above* 32^3 *the decay of kinetic energy follows a power law with a decay exponent between* 1.2 *and* 1.4*, except in the case of turbulence with a constrained length scale for which the decay exponent is* 2.1*. This is in very good agreement with experimental data and theoretical analysis where the exponent* $\approx 1.2 \rightarrow 1.4$ *unconstrained, and* 2.0 *when constrained. At a resolution of* 32^3 *the number of degrees of freedom are not sufficient to allow a turbulent flow, and velocity derivative statistics are Gaussian. The skewness of the velocity derivative is lower than existing explicit LES and Direct Numerical Simulation (DNS) simulations, but in good agreement with the most recent experimental results. There is a limited sub-inertial range with the three-dimensional Kolmogorov constant* ≈ 1.9*, also in agreement with DNS. The less dissipative nature of the third order limiter gives better skewness at a lower grid resolutions, however both give good results in terms of energy dissipation and growth of the length scales.*

1 INTRODUCTION

As current computational power does not allow Direct Numerical Simulation of complex flows, Large-eddy simulation (LES) is emerging as a viable alternative where the time dependent behaviour of the flow must be resolved. Conventional LES, where an explicit subgrid model is added to the averaged Navier Stokes equations, has been employed sucessfully in many prototype flows, however it is known to provide excessive dissipation in flows where the growth of an initially small perturbation to fully turbulent flow must

be resolved.[27,37] It has been recognised that some numerical schemes gain good results in complex flows without the explicit addition of a subgrid model.[27] This occurs when the subgrid model is implicitly designed into the limiting method of the numerical scheme, based on the observation that an upwind numerical scheme can be rewritten as a central scheme plus a dissipative term.[8] Such implicit subgrid models fall into the class of structural models, as there is no assumed form of the nature of the subgrid flow thus the subgrid model is entirely determined by the structure of the resolved flow.[41]

Excellent results have been gained in simulation of flows as varied as Rayleigh-Taylor and Richtmyer Meshkov mixing,[57,58] Free jets,[15] convection of plumes, channel flow,[15] cavity flow,[16] geophysical flows[30] and decaying turbulence.[11,12,16,38] Attempts to formalise the development of ILES numerical schemes is hindered by the inherent complexity of theoretical analysis of non-linear schemes, however, recent developments show some good agreements between truncation errors due to the numerical scheme and the required form of the subgrid terms.[29]

This paper addresses the accuracy of two limiting methods, Minmod and third order, via simulations of decaying homogeneous turbulence. This is intended as a starting point for development of ILES numerical schemes for compressible flows, by identifying *quantitatively* the strengths and weaknesses of a basic ILES simulation compared to experimental studies, DNS and previous conventional LES.

Section 2 details the numerical scheme employed, the implicit subgrid model for each of the limiting methods, and the method used to initialise a homogeneous, isotropic turbulent field. Section 3 discusses the ability of ILES solvers to predict fundamental properties of a turbulent flow field such as the skewness and flatness of the velocity derivative, the kinetic energy decay exponent, and kinetic energy spectra. Section 4 concludes this paper and discusses the areas for future development.

2 SIMULATION DETAILS

2.1 Numerical Scheme

These computations were carried out using a Finite Volume Godunov method. The flux terms are evaluated by a characteristics based Riemann solver,[10] and advanced in time using one of three different methods; semi-implicit dual time stepping,[20] 2nd order TVD Runge Kutta,[43] and 3rd order extended stability Runge-Kutta.[14] Higher order spatial accuracy is achieved using van Leer's MUSCL limiting technique.[51] The left and right states used in the calculation of the characteristics-based conservative variables are:

$$U^L_{i+1/2} = U_i + \frac{1}{4}\left[(1-k)\,\phi\left(r^L\right)(U_i - U_{i-1}) + (1+k)\,\phi\left(\frac{1}{r^L}\right)(U_{i+1} - U_i)\right] \quad (1)$$

$$U^R_{i+1/2} = U_{i+1} - \frac{1}{4}\left[(1-k)\,\phi\left(r^R\right)(U_{i+2} - U_{i+1}) + (1+k)\,\phi\left(\frac{1}{r^R}\right)(U_{i+1} - U_i)\right] \quad (2)$$

where

$$r^L = \frac{U_{i+1} - U_i}{U_i - U_{i-1}} \tag{3}$$

$$r^R = \frac{U_{i+1} - U_i}{U_{i+2} - U_i} \tag{4}$$

The slope limiter function ϕ depends upon the limiting method chosen, and the parameter k controls the different realisations of the MUSCL scheme. In this paper the following two limiters are investigated,[9,50]

$$\phi_{MM} = min\left(1, r\right), \tag{5}$$

$$\phi_{DD} = 1 - \left(1 + \frac{4r}{1+r^2}\right)\left(1 - \frac{2r}{1+r^2}\right)^2, \tag{6}$$

where the first is the Minmod limiter, and the second is a limiter which recovers full third order accuracy when $k = 1/3$.

2.2 Implicit Subgrid Models

Modified equation analysis can be used to derive the leading order truncation error of the numerical scheme, which is the implicit subgrid model.[9,40] This is gained via analysis of the spatial truncation error of the numerical scheme when applied to the Euler equations, facilitated by the use of formula manipulation software such as Mathematica. In this case the u momentum equation is examined. The spatial error terms are generated when the flux terms $\mathbf{F}\left(\mathbf{U}\right)$ are formed from limited projections of the cell centred quantities. This adds implicit dissipation which was originally developed to ensure stability of the numerical scheme. The fluxes are computed at each interface from the solution of the Reimann problem using the right and left limited variables

$$\mathbf{F_{i+1/2}} = \frac{\mathbf{1}}{\mathbf{2}}\left(\mathbf{F_L} + \mathbf{F_R}\right) - \frac{\mathbf{1}}{\mathbf{2}}\left|\mathbf{A}\right|\left(\mathbf{U_R} - \mathbf{U_L}\right), \tag{7}$$

where

$$\left|\mathbf{A}\right| = \mathbf{K}\left|\mathbf{\Lambda}\right|\mathbf{K^{-1}}, \tag{8}$$

and $\mathbf{K}$ are the right eigenvectors and $|\mathbf{\Lambda}|$ are the absolute of the flow eigenvalues. The quantities $(.)_L$ and $(.)_R$ are the values on each side of the interface. Firstly it is assumed that the primitive variables are limited, and a Taylor Series expansion is employed to give the limited value with respect to the cell centred value. Next, the fluxes at the cell interface are computed with respect to the cell centred values, using equation 7. This process is detailed in Thornber and Drikakis,[49] and the results are outlined here. The total truncation error is given as a sum of two different errors

$$T^{AV} = \left(\rho u^2 + p\right)_{exact} - \frac{1}{2}\left(\mathbf{F_L} + \mathbf{F_R}\right) \quad (9)$$

$$T^{RS} = \frac{1}{2}\left|\mathbf{A}\right|\left(\mathbf{U_R} - \mathbf{U_L}\right) \quad (10)$$

For the two given limiters the truncation errors are

$$TE^{AV}_{MM} = \frac{\Delta x^2}{12}\frac{\partial}{\partial x}\left(2M^2 u u_{xx} + p_{xx}\right) + M^2\frac{\Delta y^2}{12}\frac{\partial}{\partial y}\left(u v_{yy} + u_{yy} v\right), \quad (11)$$

$$TE^{AV}_{DD} = \frac{\Delta x^4}{30}\frac{\partial}{\partial x}\left(2M^2 u u_{xxxx} + p_{xxxx}\right) + M^2\frac{\Delta y^4}{30}\frac{\partial}{\partial y}\left(u v_{yyyy} + u_{yyyy} v\right), \quad (12)$$

and,

$$TE^{RS}_{MM} = \frac{M\Delta x^2}{4}\frac{\partial}{\partial x}\left(\rho a\left|\frac{u_{xx}}{u_x}\right| u_x + \frac{2u\hat{\gamma}}{a}\left|\frac{p_{xx}}{p_x}\right| p_x\right) + M\frac{\Delta y^2}{4}\frac{u\hat{\gamma}}{a}\frac{\partial}{\partial y}\left|\frac{p_{yy}}{p_y}\right| p_y \quad (13)$$

$$TE^{RS}_{DD} = -\frac{M\Delta x^3}{12}\frac{\partial}{\partial x}\left(\rho a u_{xxx} + \frac{2u\hat{\gamma}}{a} p_{xxx}\right) - M\frac{\Delta y^3}{6}\frac{u\hat{\gamma}}{a}\frac{\partial}{\partial y} p_{yyy} \quad (14)$$

where $(.)_x = \partial/\partial x$. This can be compared to the truncation error when spatially filtering the Euler equations, and expanding the resultant terms as a Taylor series[29]

$$TE_{Ideal} = \frac{\Delta x^2}{12}\left[M^2\left(u_x u_x\right)_x + M^2\left(u_x v_x\right)_y + \frac{p_{xxx}}{2}\right] + M^2\frac{\Delta y^2}{12}\left[\left(u_y u_y\right)_x + \left(u_y v_y\right)_y\right] \quad (15)$$

the above truncation errors demonstrate two different approaches. Firstly the limiter ϕ_{DD} characterises an approach where a high order method is used to confine the errors to high truncation order. This is intended to restrict the dissipation to high wavenumbers whilst permitting a wide range of turbulent scales to evolve unhindered. However, T^{AV} is of order M^2 whereas T^{RS} is of order M demonstrating that the Riemann solver will dominate at low Mach numbers. It is interesting to note that for Minmod there are several terms in T^{AV} which match exactly the terms in TE_{Ideal}.

2.3 Initialisation

The flow field was initialised using a method derived by Youngs and utilised in previous simulations of decaying turbulence.[57,58] The flow field has an initial kinetic energy spectrum given by

$$E(k) = u'^2\frac{k^4}{k_p^4}\sqrt{\frac{8}{k_p^2\pi}}\exp\left(-2\left(k/k_p\right)^2\right), \quad (16)$$

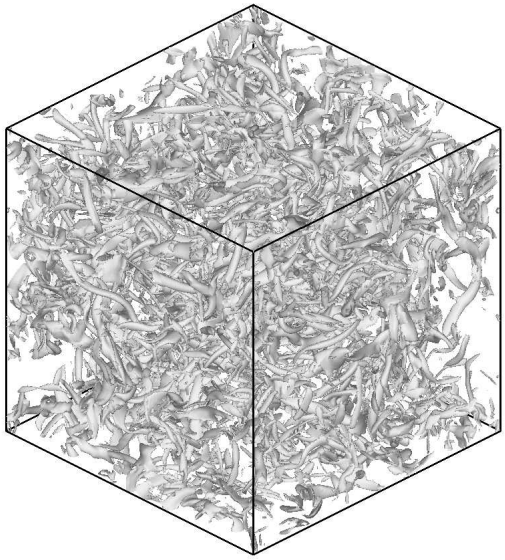

Figure 1: Iso-vorticity surfaces illustrating the worm like vortical structures in fully developed homogeneous turbulence in a 256^3

where k is the wavenumber. The peak in the energy spectrum is defined by changing the peak k_p in the exponential. Unless otherwise stated the peak of the energy spectrum was chosen at $k_p = 4$. As an indications of the level of isotropy at the larger scales the integral length has been calculated from the longitudinal and the transverse one dimensional kinetic energy spectra. Both agree to within ten percent throughout the period of the simulations, however it is observed that the simulations become increasingly more anisotropic at late times. In examining the components of the mean turbulent velocities there is a considerable anisotropy evident in the mean velocities for the 32^3, as it is extremely under-resolved. At this resolution there are only 8 cells per wavelength even at the peak of the energy spectrum. Above 32^3 the maximum mean square turbulent velocities in each direction match the mean turbulent velocity to within 6% throughout the simulation.

Figure 1 shows isosurfaces of equal vorticity magnitude taken at t=1.0 for the 256^3 case. This shows the worm like vortical structures present in the fully developed turbulent flow field. The simulations were run to t = 5.0 for all mesh resolutions, corresponding to approximately 8.0 eddy turnover times.

3 RESULTS AND DISCUSSION

3.1 Structure Functions

The velocity structure functions are typically used to quantify if the flow is turbulent, and its characteristics. These are computed as

$$S_n = \frac{\langle (\partial u/\partial x)^n \rangle}{\left\langle (\partial u/\partial x)^2 \right\rangle^{n/2}}, \tag{17}$$

The derivatives are computed using second order accurate centred differences and then averaged over all three directions in isotropic cases. The third order velocity structure function ($n = 3$) is termed 'skewness' and is directly related to enstrophy in isotropic homogenous turbulence. It is the non-Gaussian nature of the skewness of the velocity derivative which determines the dissipation rate in homogeneous isotropic turbulence. The fourth order structure function ($n = 4$) is termed the 'flatness' or 'kurtosis' and gives a measure of the probability of occurance of extreme or mild events. These, and higher order functions can also be used to measure *in vivo* the dissipation inherent in the numerical scheme. The lower the absolute value, the higher the numerical dissipation.

Sreenivasan and Antonia[46] have compiled many experimental velocity structure function measurements. The skewness appears constant at approximately 0.5 between Reynolds 10 and 1000, but increases above this threshold. The flatness increases consistently with Reynolds number, at a rate approximately $S_4 \propto 3 + 1/2Re^{0.25}$, implying that both very small and very high values of velocity derivative become more likely as the flow becomes increasingly turbulent. More recently, Kang et al[23] measured $S_3 = -0.34$ for $Re_\lambda = 720$. Computational results from DNS and LES simulations are summarised in Table 1. Table 2 details the average velocity derivative functions calculated in this study with the Minmod and third order limiters.

Figure 2 shows the time evolution of the velocity structure functions at different mesh resolutions for the third order limiter. The functions each begin at the initialised Gaussian distribution then move to non-Gaussian turbulent values. The skewness factor for the 32^3 for both limiting methods is higher than experimental values and tends rapidly back to a Gaussian distribution. The numerical dissipation of the scheme does not allow an adequate number of undamped modes to represent a turbulent flow field. Increasing the mesh resolution increases the number of degrees of freedom for the flow, thus extending the time over which the flow can be described as turbulent.

As the mesh resolution increases, the skewness increases converging towards a value of around -0.35, in good agreement with the most recent experimental results.[23] For a given mesh resolution the third order limiter gives higher skewness than the Minmod limiter as expected from a less dissipative scheme, however at resolutions of 128^3 and greater there is little different in skewness between the schemes.

The Kurtosis is lower than in previous DNS studies (See Table 1), however higher than the filtered experimental results measured in.[23] The Minmod simulations give kurtosis nearly 20% less than third order at resolutions lower than 256^3 when compared to the third order limiter due to the lower order truncation error terms. Changing the time stepping method to a third order Runge Kutta or dual time scheme, or the quantities which are limited (i.e. primitive vs. conserved variables) has an almost negligible effect on the velocity derivative functions.

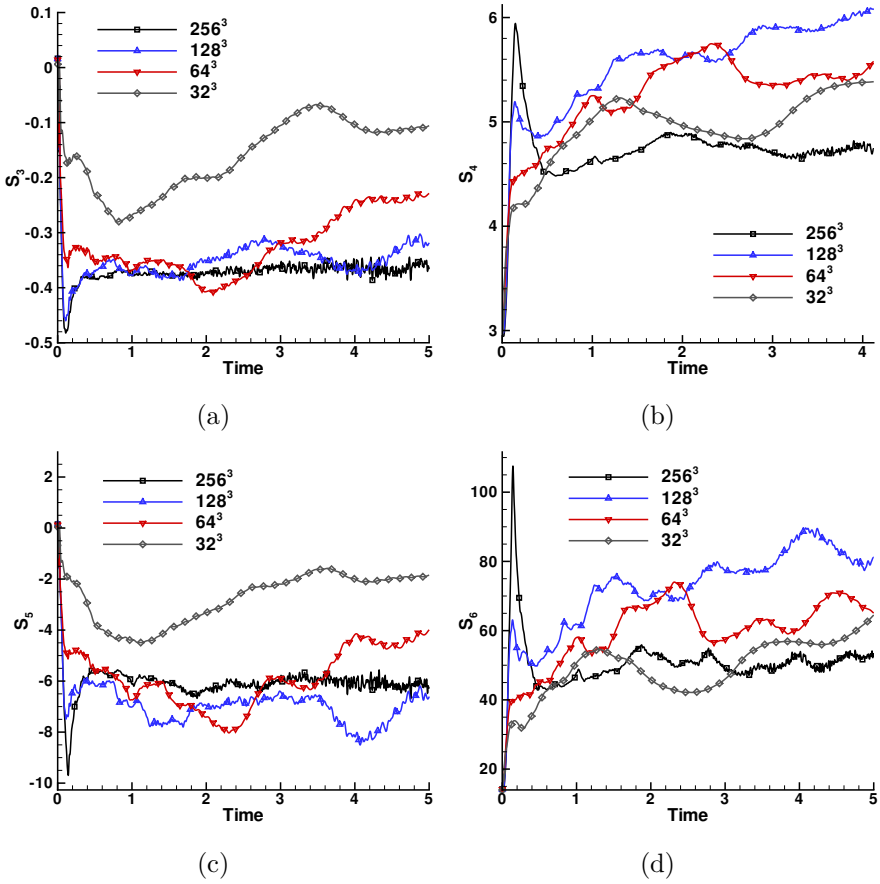

Figure 2: Variation in velocity structure functions in decaying turbulence at different mesh resolutions with the third order limiter; a) Skewness, b) Flatness or Kurtosis, c) S_5 and d) S_6

3.2 Kinetic Energy Decay Rate and Growth of the Length Scales

A numerical scheme must be able to correctly predict the rate of decay of turbulent kinetic energy to be of use in time dependent flows. It is widely accepted that the evolution of kinetic energy in homogeneous isotropic turbulence can be written as follows:[18]

$$3/2u^2 = A(t - t_0)^{-p}, \tag{18}$$

where u is the root mean square turbulent velocity, A a constant, t_0 the virtual origin in time, and p a positive constant. If the exponent is not in a physically realistic range then the simulations will rapidly decorrelate with reality. In addition to this, the growth of the energy containing scales, i.e. the integral length scale, must be represented accurately, as these eddies typically represent the dominating structures in the flow. The integral length scale is defined as

$$L_1 = \int_0^\infty f(x)dx = \pi/u^2 E_1(k=0), \tag{19}$$

where $f(x)$ is the second order velocity correlation and E_1 the longitudinal energy spectrum. The growth of the integral length scale is

$$L_1 = B\,(t - t_0)^q\,, \tag{20}$$

and q is a positive constant. Analytical theories[2,18,25,28] are based on either the Loitsyanskii or Birkhoff invariants. The Loitsyanskii invariant places the value of the decay exponents as $p = 10/7$ and $q = 2/7$ with the assumption that the low wavenumbers scale proportionally to k^4, however it has been shown that there are physical flows for which this invariant does not hold.[39] The Birkhoff invariant points to a decay exponents of $p = 6/5$ and $q = 2/5$ and assumes a k^2 scaling of the kinetic energy spectrum at low wavenumbers. More recent analysis using renormalisation group analysis by Yakhot and Orszag[55] gave $p = 1.47$, EDQNM theory gives a decay rate of 1.38,[26] and finally, Yakhot[54] proposed a new time dependent integral scale and integral invariant which gives the same decay rate as with the Loitsyanskii invariant.

Experimental results are not conclusive, however they appear to favour Birkhoff's invariant. The positioning of the virtual origin t_0 remains a key issue, as this significantly affects the decay exponent gained. Examining the excellent summary papers of Comte-Bellot and Corrsin,[6] Mohammed and LaRue[32] and Skrbek and Stalp[44] gives mixed results. Data summarised by Comte-Bellot and Corrsin[6] shows a wide range of scatter, from decay exponents of 1.0 to 1.37. They conduct more careful experiments with a level of isotropy improved by a secondary contraction gave decay rates of 1.25 with an error of 4%. Mohammed and LaRue[32] report 1.3 ± 0.02. Results from Mydlarski and Warhaft[34] give decay rates of 1.21, and more recently Kang *et al*[23] report 1.25 where the integral length scale is approximately one quarter the size of the wind tunnel. Through analyses of previous data sets and new experiments in superfluid Helium Skrbek and Stalp[44] propose that Birkhoff's invariant holds true. Previous numerical studies using conventional LES models which detail the decay exponent are listed in Table 3. In previous ILES studies Youngs[57] computed $p \approx 1.41$ using the same initialisation condition with a Lagrangian code, and Fureby and Grinstein[11] report a good match with the Comte-Bellot and Corrsin dataset.

Given an initial kinetic energy spectrum proportional to k^4 at the low wavenumbers, Loitsyanskii type decay would be expected, slowly transitioning to decay governed by the Birkhoff invariant after several eddy turnover times as the kinetic energy spectrum takes on a combined $k^2 + k^4$ spectrum at low wavenumbers. The kinetic energy decay rate is determined numerically using the kinetic energy $3/2u^2$ and the rate of change of kinetic energy $3/2\dot{u}^2$ following Youngs,[57]

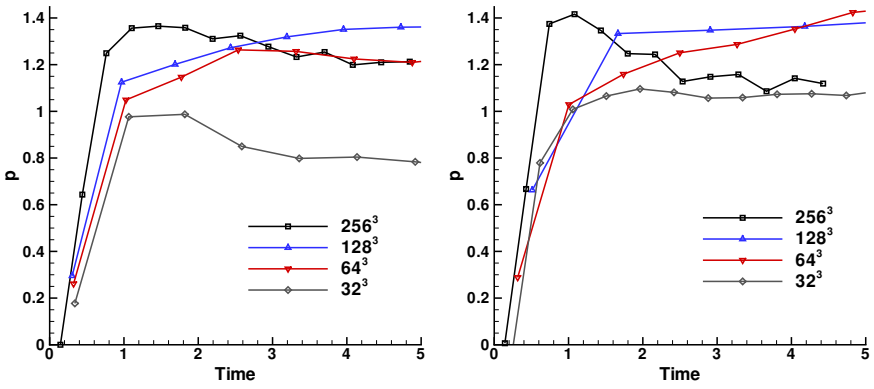

Figure 3: Variation of the kinetic energy decay exponent p for; a) Minmod limiter, b) Third order

$$-\frac{3/2\dot{u}^2}{3/2u^2} = \frac{pA(t-t_0)^{-p-1}}{A(t-t_0)^{-p}} = \frac{p}{(t-t_0)}, \tag{21}$$

which allows determination of the decay rate p with minimum influence of the virtual origin t_0.

The 32^3 simulation begins dissipating kinetic energy almost immediately, but as the resolution increases there is a longer period in which enstrophy increases and the kinetic energy is not changed significantly. The turbulent energy is being redistributed from the low wave number to the higher wave numbers, where dissipation occurs much more rapidly. The less dissipative third order limiter develops over double the peak enstrophy at each mesh resolution compared to Minmod. Tables 4 and 5 summarise the decay exponents for each mesh resolution averaged over the first 5s of decay. The coefficient B and RMS difference between an assumed 2/7 or 2/5 decay rate for the growth of the integral length scales are also detailed.

As described in the previous section the 32^3 simulations are not adequate to represent a turbulent field thus leading to unphysical decay rates. Figure 3 shows the time variation of the average kinetic energy exponent p. All simulations above 32^3 resolution demonstrate good mean decay rates where $1.2 < p < 1.4$, which decreases with decreasing mesh resolution. This decrease in decay rate is not unexpected as experimental results show that the decay rate decreases as the effective filter width is increases, as the dynamics of the larger eddies are associated with longer decay times.[23] Additional simulations of constrained turbulence where the peak of the initial spectrum is set at $k_p = 1$ gave a decay exponent of 2.12, very close to the theoretical value of 2.

Although the mean growth rate of the integral length scales detailed in Tables 4 and 5 for $1.0 < t < 5.0$ is closer in terms of RMS error to a power law of 2/7 than 2/5, it is not conclusive. Examining Figure 4 shows that the growth rate fluctuates around the

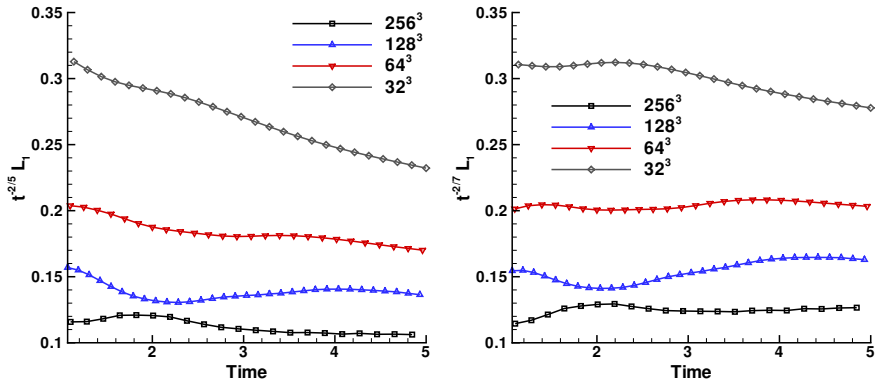

(a) (b)

Figure 4: Growth of the integral length scale rescaled by; a) $t^{-2/5}$, b) $t^{-2/7}$ in simulations using the Minmod limiter

theoretical solution throughout the decay processes, settling towards a 2/5 decay rate at the highest resolution at late times.

3.3 Spectra

The longitudinal spectrum E_1 and three dimensional energy spectrum E_3D are defined as[7,47]

$$E_1(k_1) = \frac{1}{\pi} \left\langle u_1^2 \right\rangle \int_0^\infty dx_1 f(x_1) \cos k_1 x_1, \tag{22}$$

$$E_{3D}(k) = 2\pi k^2 \phi_{ii}(k), \tag{23}$$

where f is the longitudinal velocity correlation, k_1 the wavenumber in one direction, $k = \sqrt{k_x^2 + k_y^2 + k_z^2}$, u_1 is the mean turbulent velocity in the 1 direction, and the spectrum tensor ϕ is

$$\phi_{ij}(\mathbf{k}) = \frac{1}{(2\pi)^3} \int_{-\infty}^{\infty} Q_{ij}(\mathbf{r}) \exp^{-i\mathbf{kr}} d\mathbf{r}, \tag{24}$$

where Q_{ij} is the second order correlation tensor. Figure 5 shows the compensated one dimensional and three dimensional energy spectra calculated as

$$\psi = k^{5/3} E(k) / \left\langle \epsilon \right\rangle^{2/3}. \tag{25}$$

Two straight lines are plotted at 0.5 and 1.6 which are the theoretical and experimentally measured values of the Kolomogorov constant C_k for the longitudinal and three-dimensional spectra respectively.[7,45] Note that although the spectra are all taken at time = 1.0, fully developed decay occurs earlier at lower resolutions as the starting transient is

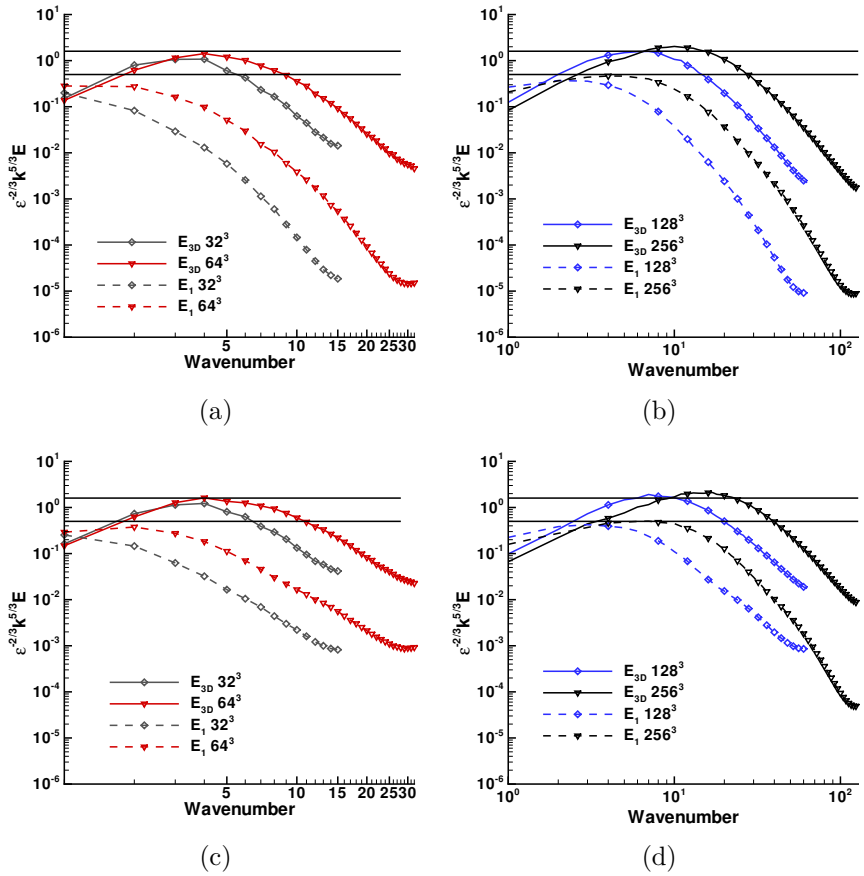

Figure 5: Longitudinal energy spectrum E_1 and three-dimensional energy spectrum E_{3D} at different mesh resolutions. The straight black lines indicate $C_k = 0.5$ and $C_k = 1.6$ respectively; a)Minmod 32^3 and 64^3, b) Minmod 128^3 and 256^3,c)Third order 32^3 and 64^3, d) Third order 128^3 and 256^3

faster due to the smaller degrees of freedom. This means that the spectra are not taken at the same effective time thus they cannot be directly compared.

It is clear from the plots that the 32^3 and 64^3 plots are too dissipative to exhibit a sub-inertial range. However, the higher resolution simulations have a sub inertial range in both the one and three dimensional spectra with $C_k(1D) \approx 0.5$ for the one dimensional spectrum and $C_k(3D) \approx 1.9$ for the three dimensional spectrum. The sub-inertial range in E_1 finishes at a lower wavenumber than in E_{3D}, consistent with observations by Monin and Yaglom[33] that the viscous cut off of the inertial range in appears earlier in E_1 than E_{3D}. The higher resolution simulations are in good agreement with the beginnings of the sub-inertial range as reported in recent high resolution spectral simulations,[13,22,56] and experimental results, especially considering that these are single time spectra from decaying turbulence not averaged from statistically stationary forced turbulence.

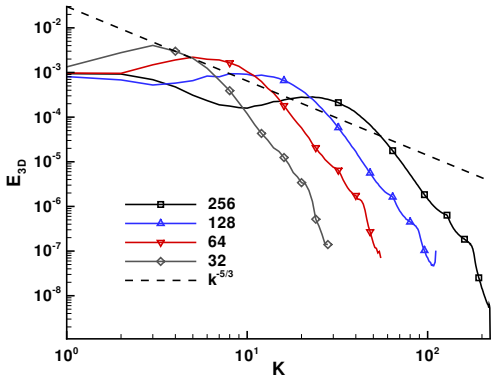

Figure 6: Three-dimensional energy spectrum E_{3D} from decaying turbulence simulations using the Superbee limiter

The extent of the inertial range is short as there is no deliberate tailoring of the limiting method towards extending the sub-inertial range. One task of limiter design is to incorporate the methodology of conventional LES modeling which has been shown to extend the sub-inertial range to the mesh cut-off.[1,19,23,53] This could be achieved by sharpening the spectral response of the limiters, or matching the truncation error of the scheme to the required subgrid model.

Note that not all limiting methods contain the correct form of dissipation to create a physically realistic spectrum. As an example of this, kinetic energy spectra from a 256^3 simulation using the Superbee limiter are shown in Figure 6. In this case the anti-diffusive nature of the limiter artificially increases the energy in the higher wavenumbers, creating unphysical behaviour, such as a decreasing integral length scale with time.

4 CONCLUSIONS

The ability of a simple ILES scheme to simulate a complex decaying turbulent field has been investigated *quantitatively* using a number of different parameters through the simulation of homogeneous turbulence in a periodic cube at Mach 0.1.

This study has demonstrated that for the present numerical scheme a simulation must be over 64^3 to allow the necessary physical attributes to be called a turbulent flow. Under this resolution both the skewness and flatness of the velocity derivative rapidly return to their Gaussian values. At higher resolutions the skewness and kurtosis of the velocity structure functions converge to around -0.35 and ≈ 45, lower than the majority of experimental data indicating that there is too much dissipation at the higher wavenumbers, however they are in good match with the most recent wind tunnel data.

The mean kinetic energy decay rate exponent is between 1.2 and 1.4 for all resolutions greater than 32^3, matching experimental data and theory very well. For turbulence with a constrained length scale the theoretical decay exponent is 2, and simulations with the peak of the spectrum at the first mode gave a decay rate of 2.1. Additionally, the ILES schemes

predict the growth of the energy containing scales with reasonable accuracy compared to theoretical results predicted via the application of the Loitsyanskii and Birkhoff invariants.

The spectra show a limited Kolmogorov sub-inertial range with a three dimensional Kolmogorov coefficient $C_k \approx 1.9$. This is slightly higher than the theoretical value of ≈ 1.6 but consistent with the beginning of a sub-inertial range shown in very high resolution DNS studies.

Numerically, changing the time stepping method from semi-implicit dual time stepping to the Runge Kutta schemes had very little noticable effect on the statistics measured. The third order limiter performed better overall in that it is less dissipative thus allowing a slightly longer sub-inertial range, and higher enstrophy at the same mesh resolution. This is due to the higher order accuracy of the numerical scheme, which appears to compensate for the fact that the subgrid stresses are not proportional to the square of the cell length. It is also noted that spatially limiting the primitive variables instead of the conserved variables increases the dissipation rate, however it does not appear to influence the velocity structure functions.

This work has demonstrated that a simple ILES scheme can successfully predict key features of a turbulent flow field such as the kinetic energy decay rate and growth of the integral length scales. It has also highlighted weaknesses, such as the limited sub-inertial range present in the kinetic energy spectra. Future work will focus around two themes; First is the design of limiters which mimic the behaviour of the existing subgrid models and thus are constructed with some assumed structure of the subgrid scales (i.e. a type of 'functional ILES'), the second step is to build on the strength of ILES, i.e. the ability to allow the growth of small scale perturbations at low mesh resolution in flows of mixed compressible/incompressible nature, such as shock-turbulence interaction.

5 ACKNOWLEDGEMENTS

The authors would like to thank Robin Williams, David Youngs and Anthony Weatherhead (AWE, Aldermaston) and Evgeniy Shapiro (Fluid. Mechanics and Computational Science Group, Cranfield University) for their advice and suggestions whilst developing the computer code.The computations were carried out on the Cambridge-Cranfield High Performance Computing Facility. This work is supported by an EPSRC-AWE PhD Case award.

REFERENCES

[1] R. Anderson and C. Meneveau. Effects of the similarity model in finite-difference les of isotropic turbulence using a lagrangian dynamic mixed model. *Flow Turbul. Combust.*, 62:201–225, (1999).

[2] G. Birkhoff. Fourier synthesis of homogeneous turbulence. *Commun. Pure Appl. Math.*, 7:19–44, (1954).

[3] D. Carati, S. Ghosal, and P. Moin. On the representation of backscatter in dynamic localization models. *Phys. Fluids*, 7(3):606–616, (1995).

[4] S. Chen, G.D. Doolen, R.H. Kraichnan, and Z-S. She. On statistical correlations between velocity increments and locally averaged dissipation in homogeneous turbulence. *Phys. Fluids A*, 5(2):458–463, (1992).

[5] S.G. Chumakov and C.J. Rutland. Dynamic structure subgrid-scale models for large eddy simulation. *Int. J. Numer. Meth. Fl.*, 47:911–923, (2005).

[6] G. Comte-Bellot and S. Corrsin. The use of a contraction to improve the isotropy of grid generated turbulence. *J. Fluid Mech.*, 25:657–682, (1966).

[7] P.A. Davidson. *Turbulence - An Introduction for Scientists and Engineers*. Oxford University Press, (2004).

[8] D.Drikakis. Advances in turbulent flow computations using high-resolution methods. *Prog. Aerosp. Sci.*, 39:405–424, (2003).

[9] D. Drikakis and W. Rider. *High-Resolution Methods for Incompressible and Low-Speed Flows*. Springer Verlag, (2004).

[10] A. Eberle. Characteristic flux averaging approach to the solution of euler's equations. Technical report, VKI Lecture Series, (1987).

[11] C. Fureby and F.F. Grinstein. Large eddy simulation of high-reynolds-number free and wall-bounded flows. *J. Comp. Phys.*, 181:68–97, (2002).

[12] C. Fureby, F. Tabor, H.G. Weller, and A.D. Gosman. A comparative study of subgrid scale models in homogeneous isotropic turbulence. *Phys. Fluids*, 9(5):1416–1429, (1997).

[13] T. Gotoh, D. Fukayama, and T. Nakano. Velocity field statistics in homogeneous steady turbulence obtained using a high resolution direct numerical simulation. *Phys. Fluids*, 14(3):1065–1081, (2002).

[14] S. Gottlieb and C-W Shu. Total variation diminishing runge-kutta schemes. *Math. Comput.*, 67(221):73–85, (1998).

[15] F.F. Grinstein and C. Fureby. Recent progress on miles for high reynolds number flows. *J. Fluid Eng.- T. ASME*, 848:848–861, (2002).

[16] M. Hahn and D. Drikakis. Large eddy simulation of compressible turbulence using high-resolution method. *Int. J. Numer. Meth. Fl.*, 49:971–977, (2005).

[17] N.E.L. Haughen and A. Brandenburg. Inertial range scaling in numerical turbulence with hyperviscosity. *Phys. Rev. E*, 70:026405, (2004).

[18] J.O. Hinze. *Turbulence*. McGraw-Hill, 2 edition, (1975).

[19] T.J.R. Hughes, L. Mazzei, and A.A. Oberai. The multiscale formation of large eddy simulation: Decay of homogeneous isotropic turbulence. *Phys. Fluids*, 13(2):505–512, (2001).

[20] A. Jameson. Time dependent calculations using multigrid, with applications to unsteady flows past airfoils and wings. *AIAA 91-1596*, (1991).

[21] J. Jimenez, A.A. Wray, P.G. Saffman, and R.S. Rogallo. The structure of intense vorticity in isotropic turbulence. *J. Fluid Mech.*, 255:65–90, (1993).

[22] Y. Kaneda, T. Ishihara, M. Yokokawa, K. Itakura, and A. Uno. Energy dissipation rate and energy spectrum in high resolution direct numerical simulations of turbulence in a periodic box. *Phys. Fluids*, 15(2):L21–L24, (2003).

[23] H.S. Kang, S. Chester, and C. Meneveau. Decaying turbulence in an active-grid-generated flow and comparisons with large-eddy simulation. *J. Fluid Mech.*, 480:129–160, (2003).

[24] R.M. Kerr. Higher order derivative correlations and the alignment of small scale structures in isotropic turbulence. *J. Fluid Mech.*, 153:31–58, (1985).

[25] A.N. Kolmogorov. The local structure of turbulence in an incompressible fluid at very high reynolds numbers. *Dokl. Akad. Nauk. SSSR*, 30:299, (1941).

[26] M. Lesieur. *Turbulence in Fluids*. Kluwer Academic Publishers, (1987).

[27] M. Lesieur and O. Metais. New trends in large-eddy simulations of turbulence. *Annu. Rev. Fluid Mech.*, 28:45–82, (1996).

[28] L.G. Loitsyanskii. *Mechanics of Liquids and Gases*. Pergamon Press, (1966).

[29] L.G. Margolin, W.J. Rider, and F.F. Grinstein. Modeling turbulent flow with implicit les. *J. Turbul.*, 7(15):1–27, (2006).

[30] L.G. Margolin, P.K. Smolarkiewicz, and Z. Sorbjan. Large-eddy simulations of convective boundary layers using nonoscillatory differencing. *Physcica D*, 133:390–397, (1999).

[31] O. Metais and M. Lesieur. Spectral large-eddy simulation of isotropic and stably stratified turbulence. *J. Fluid Mech.*, 239:157–194, (1992).

[32] M.S. Mohammed and J.C. LaRue. The decay power law in grid-generated turbulence. *J. Fluid Mech.*, 219:195–215, (1990).

[33] A.S. Monin and A.M. Yaglom. *Statistical Fluid Mechanics, Mechanics of Turbulence*, volume 2. MIT Press, (1975).

[34] Z. Mydlarski, L.and Warhaft. On the onset of high-reynolds grid-generated wind tunnel turbulence. *J. Fluid Mech.*, 320:331–368, (1996).

[35] S.A. Orzag and G.S. Patterson. Numerical simulation of three-dimensional homogeneous isotropic turbulence. *Phys. Rev. Lett.*, 28:76–79, (1972).

[36] R. Panda, V. Sonnad, and E. Clementi. Turbulence in a randomly stirred fluid. *Phys. Fluids A*, 1(6):1045–1053, (1989).

[37] S.B. Pope. *Turbulent Flows*. Cambridge University Press, (2000).

[38] D.H. Porter, P.R. Woodward, and A. Pouquet. Inertial range structures in decaying compressible turbulent flows. *Phys. Fluids*, 10(1):237–245, (1998).

[39] I. Proudman and W.H. Reid. On the decay of a normally distributed and homogeneous turbulent velocity field. *Philos. Trans. R. Soc. London*, 247A:163–189, (1954).

[40] W.J. Rider and L. Margolin. From numerical analysis to implicit subgrid turbulence modelling. *AIAA 2003-4101*, (2003).

[41] P. Sagaut. *Large Eddy Simulation for Incompressible Flows*. Springer Verlag, (2001).

[42] R. Samtaney, D.I. Pullin, and B. Kosovic. Direct numerical simulation of decaying compressible turbulence and shocklet statistics. *Phys. Fluids*, 13(5):1415–1430, (2001).

[43] C.-W. Shu. Total-variation-diminishing time discretizations. *SIAM J. Sci. Stat. Comp.*, 9:1073–1084, (1988).

[44] L. Skrbek and S.R. Stalp. On the decay of homogeneous isotropic turbulence. *Phys. Fluids*, 12(8):1997–2019, (2000).

[45] K.R. Sreenivasan. On the universality of the kolmogorov constant. *Phys. Fluids*, 7(11):2778–2784, (1995).

[46] K.R. Sreenivasan and R.A. Antonia. The phenomenology of small-scale turbulence. *Annu. Rev. Fluid Mech.*, 29:435–472, (1997).

[47] H. Tennekes and J.L. Lumley. *A First Course in Turbulence*. MIT Press, (1972).

[48] M. Terracol and P. Sagaut. A multilevel-based dynamic approach for subgrid-scale modeling in large-eddy simulation. *Phys. Fluids*, 15(12):3671–3682, (2003).

[49] B. Thornber and D. Drikakis. Iles of shock waves and turbulent mixing using high resolution riemann solvers and tvd methods. In *ECCOMAS 2006,Minisymposia on Large Eddy Simulation : Theory and Applications*, (2006).

[50] E.F. Toro. *Riemann Solvers and Numerical Methods for Fluid Dynamics*. Springer-Verlag, (1997).

[51] B. van Leer. Towards the ultimate conservative difference scheme.iv. a new approach to numerical convection. *J. Comput. Phys.*, 23:276–299, 1977.

[52] A. Vincent and M. Meneguzzi. The spatial structure and statistical properties of homogeneous turbulence. *J. Fluid Mech.*, 225:1–20, (1991).

[53] L. Wang, S. Chen, J.G. Brasseur, and J.C. Wyngaard. Examination of hypotheses in the kolmogorov refined turbulence theory through high-resolution simulations. part1. velocity field. *J. Fluid Mech.*, 309:113–156, (1996).

[54] V. Yakhot. Decay of three-dimensional turbulence at high reynolds numbers. *J. Fluid Mech.*, 505:87–91, (2004).

[55] V. Yakhot and S.A. Orszag. Renormalization group analysis of turbulence. *Phys. Rev. Lett.*, 57:1722–1725, (1986).

[56] M. Yokokawa, K. Itakura, A. Uno, T. Ishihara, and Y. Kaneda. 16.4 tflops direct numerical simulation of turbulence by a fourier spectral method on the earth simulator. In *Proceedings of the 2002 ACM/IEEE conference on Supercomputing*, pages 1–17, (2002).

[57] D.L. Youngs. Three-dimensional numerical simulation of turbulent mixing by rayleigh-taylor instability. *Phys. Fluids A*, 3(5):1312–1320, (1991).

[58] D.L. Youngs. Application of miles to rayleigh-taylor and richtmyer-meshkov mixing. *AIAA-2003-4102*, (2003).

Table 1: Velocity structure functions computed from DNS - for brevity only the results for the maximum Re_λ simulated for each source are listed. Simulations up to the separating line are DNS, the remaining are LES.

Source	Re_λ	S_3	S_4
Orzag[35]	45	-0.47	-
Kerr[24]	83	-0.51	-
Panda et al.[36]	64	-0.4	4.05
Vincent and Meneguzzi[52]	150	-0.5	5.9
Metais and Lesieur[31]	< 51	-0.58	4.31
Chen et al.[4]	202	-0.44	-
Jimenez et al.[21]	168	-0.52	6.1
Wang et al.[53]	195	-0.54	6.7
Samtaney et al.[42]	175	-0.45	-
Gotoh et al.[13]	460	-0.55	7.91
Carati et al.[3]	∞	-0.4	2.73
Fureby et al.[12]	248	-	3.6
Anderson and Meneveau[1]	< 71	-0.4	-
Hughes et al.[19]	∞	-0.22	-
Kang et al.[23]	720	-0.42	-
Gaussian	-	0.00	3.00

Table 2: Velocity structure functions using the Minmod limiter, LP = limiting primitive variables, RK3 with 3rd order TVD Runge-Kutta,DT indicates a simulation with 2nd order dual time stepping scheme

	Minmod		Third order	
Mesh Resolution	S_3	S_4	S_3	S_4
32^3	-0.08	4.09	-0.14	5.17
64^3	-0.22	4.07	-0.31	5.49
128^3	-0.31	4.34	-0.34	5.8
256^3	-0.34	4.56	-0.36	4.74
256^3 LP	-0.33	4.59	-	-
256^3 RK3	-0.34	4.56	-	-
256^3 DT	-	-	-0.37	4.57

Table 3: Kinetic energy decay exponents using conventional LES modelling

Source	-p
Metais and Lesieur[31]	1.37
Carati et al.[3]	$1.17 \rightarrow 1.27$
Wang et al.[53]	1.81
Anderson and Meneveau[1]	< 1.25
Hughes et al.[19]	2
Terracol and Sagaut[48]	1.97
Haughen and Brandenburg[17]	1.25
Chumakov and Rutland[5]	1.3

Table 4: Turbulent kinetic energy decay rate and the RMS error when fitting the growth of the integral length scale using two power laws for the Minmod limiter. LP = limiting primitive variables, RK3 with 3rd order TVD Runge-Kutta

Mesh Resolution	p	B $(q = 2/7)$	B $(q = 2/5)$
32^3	0.83	0.30 ± 0.004	0.27 ± 0.007
64^3	1.26	0.21 ± 0.0002	0.18 ± 0.003
128^3	1.34	0.15 ± 0.002	0.12 ± 0.0004
256^3	1.28	0.12 ± 0.0004	0.11 ± 0.001
256^3 LP	1.40	0.12 ± 0.0007	0.11 ± 0.003
256^3 RK3	1.29	0.12 ± 0.0001	0.11 ± 0.002

Table 5: Turbulent kinetic energy decay rate and the RMS error when fitting the growth of the integral length scale using two power laws for the third order limiter. DT indicates a simulation with 2nd order dual time stepping scheme

Mesh Resolution	p	B $(q = 2/7)$	B $(q = 2/5)$
32^3	1.1	0.24 ± 0.0006	0.21 ± 0.002
64^3	1.39	0.16 ± 0.002	0.14 ± 0.004
128^3	1.34	0.11 ± 0.00007	0.10 ± 0.002
256^3	1.22	0.1 ± 0.003	0.09 ± 0.004
256^3 DT	1.34	0.1 ± 0.002	0.1 ± 0.0007